Investigation on the structural and thermal behaviors of PAMAM dendrimer encapsulated-Au nanoparticles of different sizes

ARTICLE *in* INDUSTRIAL & ENGINEERING CHEMISTRY RESEARCH · OCTOBER 2015

Impact Factor: 2.59 · DOI: 10.1021/acs.iecr.5b02382

I&EC research
Industrial & Engineering Chemistry Research

Article

pubs.acs.org/IECR

Investigation on the Structural and Thermal Behaviors of Poly(amidoamine) Dendrimer-Encapsulated Au Nanoparticles of Different Sizes

Hui-Lung Chen,[†,#] Chia-Hao Su,[‡,#] Shin-Pon Ju,[*,§,∥] Ying-Chen Chuang,[§] Po-Yu Yang,[§] Hsing-Yin Chen,[∥] and Hsin-Tsung Chen[⊥]

[†]Department of Chemistry and Institute of Applied Chemistry, Chinese Culture University, Taipei 111, Taiwan
[‡]Institute for Translational Research in Biomedicine, Kaohsiung Chang Gung Memorial Hospital, Kaohsiung 833, Taiwan
[§]Department of Mechanical and Electro-Mechanical Engineering, National Sun Yat-sen University, Kaohsiung 80424, Taiwan
[∥]Department of Medicinal and Applied Chemistry, Kaohsiung Medical University, Kaohsiung 80708, Taiwan
[⊥]Department of Chemistry, Chung Yuan Christian University, Chungli District, Taoyuan City 32023, Taiwan

ABSTRACT: The dynamical and thermal behaviors of Au nanoparticle (AuNP) and fourth generation poly(amidoamine) dendrimer (G4 PAMAM) of the dendrimer-encapsulated Au nanoparticle system under the dry environment were investigated by the molecular dynamics (MD) simulation. The consistent valence force field (CVFF) was used to describe the interaction of the G4 PAMAM dendrimer and the interaction between the dendrimer and the AuNP. The many-body tight-binding potential was adopted to describe the atomic interaction between the Au atoms of an AuNP. Three AuNPs, Au_{116}, Au_{201}, and Au_{405}, with the diameters of 1.45, 1.8, and 2.3 nm were concerned, respectively. Au_{116} and Au_{201} are nearly completely covered by G4 PAMAM dendrimer, but the branching chains of the dendrimer are no longer able to wrap around the Au_{405}.The conformation of G4 PAMAM dendrimer still possesses its unique spherical structure after encapsulating the AuNP, and the irregularity of the outer surface decreases as the size of the AuNP increases. For the thermal stability, it was found that the PAMAM dendrimer conducts thermal expansion when temperature increases from 298 K to about 600 K. At temperatures higher than 600 K, the dendrimer moves relative to the AuNP. It also can be seen that the melting points of PAMAM dendrimer-encapsulated AuNPs increase significantly when compared to bare AuNPs of the same size. This study would help us to clarify the characteristics and phenomenon of PAMAM−AuNP composites, and these theoretical insights thus provide valuable information for future strategic design of new high-performance catalysts and nanosensors.

1. INTRODUCTION

The progress of nanotechnology has provided metal nanoparticles much wider applications in the fields of catalysis, optics, magnetic and biomedical sciences in recent years.[1−3] Among metal nanoparticles, the Au nanoparticle (AuNP) is the most popular, because AuNPs of different sizes possess different remarkable optical and electrical properties.[4] In addition, gold nanostructures also exhibit excellent biocompatibility,[5] which suggests their great potential for biological applications. For a catalyzing reaction, it has been proven that AuNPs with diameters smaller than 5 nm display efficient catalytic activity for several chemical reactions, such as the oxidation of alcohol and the reduction of 4-nitrophenol,[6−8] revealing the significantly size-dependent properties for AuNPs. Consequently, preventing a single AuNP from aggregating to form a larger AuNP is a critical step to promote these applications.

The most efficient approach is to synthesize AuNPs from Au atoms within the organic ligands, polymers, and dendrimers, which are viewed as the templates or stabilizers to produce AuNPs with sizes within a certain range.[9−11] Comparing with other stabilizers, the dendrimer contains modifiable surface groups, controllable molecular structure, and biocompatibility that give rise to many potential applications. These materials possess a number of generations and functional groups. Each new generation of material effectively doubles the number of end groups and branch points, as well as increasing the size. Recently, dendrimers have been widely used as stabilizers of AuNPs and other metallic nanoparticles.[12−14] Among all kinds of dendrimers, poly(amidoamine) (PAMAM) dendrimers are the most frequently studied for encapsulating nanoparticles because their repetitively branched subunits of amide and amine functionality make them suitable for biological applications.[15−17]

Many experimental approaches have been conducted to investigate the properties of PAMAM-encapsulated AuNPs, which are primarily applied to catalysis and biomedical sciences. For example, Li et al.[8] investigated the applications of Au nanoparticles encapsulated in a PAMAM−silica organic−inorganic hybrid composite, with results showing that the composite can effectively catalyze the oxidation of various alcohols under mild conditions. Wang et al.[18] synthesized the dendrimer-encapsulated AuNPs and used them as carriers of thiolated anticancer drugs, and the results showed excellent

Received: June 30, 2015
Revised: September 29, 2015
Accepted: October 30, 2015
Published: October 30, 2015

DOI: 10.1021/acs.iecr.5b02382
Ind. Eng. Chem. Res. 2015, 54, 11560−11567

biocompatibility on several cell lines. Shi et al.[19] present a general approach for the targeting and imaging of cancer cells using dendrimer-entrapped gold nanoparticles. In dry environments, PAMAM-encapsulated AuNPs have been developed for nanosensors. Crespilho et al.[20] used PAMAM dendrimers as stabilizers for producing immobilized AuNP layers on indium tin oxide (ITO) substrates, by which AuNP layers can enhance the charge transfer rate and mediate redox substances for sensors. Su et al.[21] fabricated a low-humidity sensor by coating the PAMAM-encapsulated AuNP thin film on a quartz crystal microbalance. The extent of AuNP stabilization within the PAMAM dendrimer is a critical factor to influence efficiency of the low-humidity sensor. Previously experimental studies indicated that the PAMAM/AuNP composites are stable and have been applied widely both in solvation and dry environment.[20,21]

Furthermore, after the dendrimer−metal nanoparticles composites are completely synthesized, dendrimers can be removed by calcination to leave behind just the metallic nanoparticles. Kuhn et al.[22] synthesized dendrimer-stabilized Pd/Au nanoparticles and removed the dendrimer by calcination. In addition, the resulting materials are highly active catalysts in ethylene acetoxylation to the vinyl acetate monomer. Scott et al.[23] fabricated titania-supported Au and Pd by using PAMAM dendrimer-encapsulated nanoparticle precursors. During the preparation, the composite was calcined up to 500 °C, and only the bare metal nanoparticles remained after the dendrimers were completely thermally degraded. Therefore, the thermal stability of dendrimer-encapsulated metal nanoparticles is also an important topic for metal nanoparticles of different sizes.

Although the approximate size distribution of PAMAM-encapsulated AuNPs can be observed by experiment, some drawbacks may still exist in the experimental approach. For example, the assembly mechanism of the PAMAM dendrimer and AuNP is difficult to observe due to the limitations of the experimental equipment at such a small scale. The dynamical behaviors of AuNP and PAMAM dendrimer are also difficult to explore by direct experimental approach during the temperature elevation process that degrades the dendrimer. Consequently, numerical methods must be used to retrieve the information beyond experimental limitations. Among these numerical methods, molecular dynamics (MD) simulation is a powerful tool facilitating the investigation of the assembling mechanism of polymer and nanoparticle at the atomic level.[24−28] For PAMAM-encapsulated AuNPs, Mandal et al.[29] used fully atomistic classical molecular dynamics simulations to obtain the interaction of AuNPs and dendrimer-AuNP composites, with results showing that the adsorption of the dendrimer on the surface of the AuNP strongly alters the interaction between the nanoparticles.

Though the interactions between dendrimers and AuNPs have been investigated, there is still a lack of numerical research on their detailed conformations, surface characteristics, and the thermal stability of PAMAM−AuNP composites. In this paper, molecular dynamics simulations were performed to predict the conformation and the thermal stability of a PAMAM dendrimer encapsulating AuNPs of different sizes. The fourth generation (G4) PAMAM dendrimers were chosen because they are most frequently used as stabilizers of nanoparticles. The solvent-free simulation was achieved to give a clear investigation of the assembly arrangement of AuNP covered by the G4 PAMAM in a dry environment. Furthermore, the simulation along with the heating process reflects the thermal affection of the PAMAM-encapsulated AuNPs.

2. SIMULATION MODEL

Three different sizes of Au nanoparticles are studied in this work. Figure 1a−c shows the AuNP at the different diameters

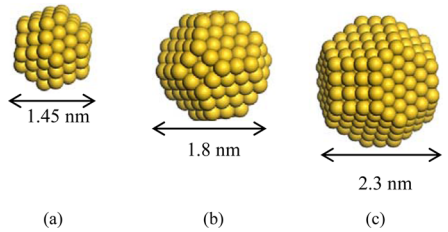

Figure 1. Different sizes of AuNP: (a) Au_{116}, (b) Au_{201}, and (c) Au_{405}.

of 1.45, 1.8, and 2.3 nm, respectively, which are labeled as Au_{116}, Au_{201}, and Au_{405}. The sizes of AuNP are in accordance with the experimental results of the PAMAM−AuNP composites.[18,20] The initial structures of the AuNPs covered by the G4 PAMAM dendrimer are shown in Figure 2. Since the

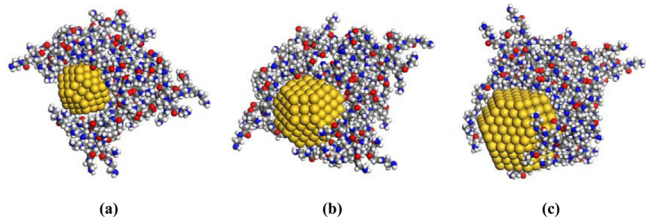

Figure 2. Initial conformation of PAMAM−AuNP composites: (a) G4 PAMAM/Au_{116}, (b) G4 PAMAM/Au_{201}, and (c) G4 PAMAM/Au_{405}.

structure of the PAMAM dendrimer in gaseous phase is more compact than in solvent, the AuNPs may not be encapsulated completely if they are just placed beside the dendrimer. Therefore, the AuNPs are placed nearby the center of the dendrimer, which causes the side chains of the dendrimer to wrap around it. The pseudo atom with a huge van der Waals radius is applied to repulse the branches of the dendrimer and reserve a space to place the AuNPs. All of the 3D molecular models are constructed by Materials Studio 5.5.[30]

In this study, molecular dynamics simulation was carried out by using the LAMMPS (Large-scale Atomic/Molecular Massively Parallel Simulator,[31] and a hybrid potential system was applied in the simulation model to improve the accuracy. The CVFF (consistent valence force field)[32] is used to describe the interactions of the PAMAM dendrimer. The tight-binding potential method is used to calculate the atomic interactions between the Au atoms of the AuNPs. This model sums the band energy, which is characterized by the second moment of the d-band density of state, and a pairwise potential energy of the Born-Mayer type,[33] i.e.,

$$E_i = -\left\{\sum_j \xi^2 \exp\left[-2q\left(\frac{r_{ij}}{r_0} - 1\right)\right]\right\}^{1/2} + \sum_j A \exp\left[-p\left(\frac{r_{ij}}{r_0} - 1\right)\right] \quad (1)$$

DOI: 10.1021/acs.iecr.5b02382
Ind. Eng. Chem. Res. 2015, 54, 11560−11567

where ξ is the effective hopping integral, r_{ij} is the distance between atoms i and j, and r_0 is the first-neighbor distance. The parameters A, p, q, and ξ are determined from the experimental data relating to the cohesive energy, the lattice parameter, the bulk modulus, and the shear elastic constants, respectively. The tight-binding potential parameters of the Au−Au interactions adopted in the present study are listed in Table 1. The

Table 1. Au Tight-Binding Potential Parameters

	A (eV)	ξ (eV)	p	q	r_0 (Å)
Au[33]	0.189	1.744	10.40	3.87	2.88

interaction between the AuNP and PAMAM dendrimer is adjusted by the optimized CVFF force field, which was developed by Heinz et al.[34] The optimized CVFF force field can precisely simulate metal and hybrid interfaces with organic, inorganic, and biological compounds, as well as mechanical properties in quantitative (<0.1%) to good qualitative (25%) agreement with experiment under ambient conditions.

During the simulation, the conjugate gradient method was used to optimize the structure, followed by a simulated annealing process performed from the initial temperature (700 K) to the target temperature (298 K), with a decreasing rate of 50 K per 100 ps. In order to ensure that the system achieved an equilibrium state, when the system reached the target temperature, a total simulation time of 2 ns was continued by NVT ensemble with time step of 1 fs. The Nosé−Hoover method was used as a thermostat, the van der Waals interactions were cutoff at 12.5 Å, and the long-range electrostatic interactions were evaluated using the Ewald summation.

3. RESULTS AND DISCUSSION

The present study focuses on realizing the structural properties and the thermal stability of AuNPs covered by G4 PAMAM dendrimer in a dry environment. The radius of gyration, the asphericity parameter, and the radius density function were used to understand the structural behaviors of the G4 PAMAM−AuNP composites.

Figure 3 shows the final conformations of G4 PAMAM/AuNPs after the MD simulations at 298 K. For G4 PAMAM/

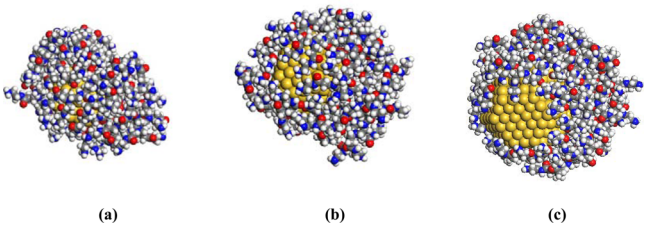

Figure 3. Stable conformations of PAMAM−AuNP composites: (a) G4 PAMAM/Au_{116}, (b) G4 PAMAM/Au_{201}, and (c) G4 PAMAM/Au_{405}.

Au_{116}, the nanoparticle is completely covered by the dendrimer, as shown in Figure 3a, implying that AuNPs smaller than this size can be effectively stabilized by the G4 PAMAM dendrimer. For nanoparticle sizes larger than that of Au_{116}, shown in Figure 3b,c, it can be seen that some surface atoms of the AuNPs are exposed, and the exposed surface atoms apparently increase with the increasing AuNP size. It was proposed that the AuNPs with more exposed surface Au atoms may lead to aggregation with the exposed parts of other AuNPs to form larger AuNPs or stabilization by being covered by another G4 PAMAM dendrimer. Table 2 summarizes the PAMAM coverage ratios of Au_{116}, Au_{201}, and Au_{405}, which are 100%, 95.08%, and 84.31%, respectively.

Table 2. Coverage Ratio of Stabilized Au Nanoparticles by G4 PAMAM Dendrimer

	G4 PAMAM/Au_{116}	G4 PAMAM/Au_{201}	G4 PAMAM/Au_{405}
coverage ratio	100%	95.08%	84.31%

Since the extent of AuNP encapsulation by the G4 PAMAM dendrimer significantly depends on the size of the AuNP, better coverage is likely if the shapes of the dendrimer are different from pristine. The radius of gyration R_g can be used to describe the expansion or contraction of a polymer chain, as well as indicating the polymer dimension. The definition of R_g can be expressed by eq 2:

$$R_g^2 = \frac{1}{M}\langle[\sum_{i=1}^{N} m_i|r_i - r_c|]\rangle \quad (2)$$

where M is the total mass of the dendrimer; m_i is the mass of the ith atom; r_c stands for the center of mass of the dendrimer; and r_i indicates the coordinates of atom i. For a molecule, a larger value of R_g indicates a more expansive structure, whereas a smaller value of R_g shows the opposite. Table 3 lists the R_g

Table 3. Radius of Gyration of Dendrimer-Encapsulated AuNPs for G4 PAMAM Dendrimer of Different Sizes

	R_g (Å)		
	this work	Maiti[35]	Lee[36]
G4 PAMAM dendrimer	14.21	14.50	14.80
G4 PAMAM/Au_{116}	14.59	-	-
G4 PAMAM/Au_{201}	14.99	-	-
G4 PAMAM/Au_{405}	15.96	-	-

values of three PAMAM dendrimers with AuNPs as well as a pristine dendrimer in vacuum after the MD simulation at room temperature, along with those reported in previous MD results in vacuum.[35,36] Our simulation R_g results for the dendrimer is 2% and 4% smaller than those of Maiti's and Lee's simulation studies, indicating our simulation model can basically reflect the structural properties of the PAMAM dendrimer.

In Table 3, one can see that PAMAM/Au_{116} has a R_g value relatively close to that of pristine PAMAM dendrimer, indicating the interior cavity formed by the pristine PAMAM dendrimer is large enough to encapsulate the whole AuNP without significantly changing the conformation of the dendrimer. PAMAM/Au_{201} and PAMAM/Au_{405} display larger R_g values than those of PAMAM/Au_{116} and pristine dendrimer. This result implies that the size of the AuNP considerably affects the conformation of the dendrimer once the AuNP becomes larger than a certain size. For AuNPs with the sizes larger than 2 nm, the dendrimer cavity can only partially encapsulate the AuNP and forces the extension of the dendrimer end branch, resulting in an increase in the R_g value.

To observe the conformation change of the PAMAM dendrimer after encapsulating AuNPs, the asphericity param-

DOI: 10.1021/acs.iecr.5b02382
Ind. Eng. Chem. Res. 2015, 54, 11560−11567

Table 4. Asphericity Parameter of AuNPs of Different Sizes Covered by G4 PAMAM Dendrimer

	G4 PAMAM dendrimer	G4 PAMAM/Au_{116}	G4 PAMAM/Au_{201}	G4 PAMAM/Au_{405}
δ	0.046	0.043	0.021	0.041

eter (δ) was used. This parameter is defined as the following equation:[37]

$$\delta = 1 - 3\left(\frac{I_2}{I_1^2}\right) \quad (3)$$

where the gyration tensor I_j is determined by the three eigenvalues R_{g1}, R_{g2}, and R_{g3} of R_g^2, where $I_1 = R_{g1} + R_{g2} + R_{g3}$, $I_2 = R_{g1}R_{g2} + R_{g2}R_{g3} + R_{g3}R_{g1}$, and $I_3 = R_{g1}R_{g2}R_{g3}$. Values of δ close to 0 indicate that a molecule arranges in a perfect sphere, whereas the configuration of the molecule is rod-like when δ = 1. Table 4 shows the asphericity parameters of the PAMAM dendrimer with the AuNPs of different nanoparticle sizes and the pristine dendrimer. The asphericity parameter of G4 PAMAM dendrimer in vacuum is about 0.046, which is in good agreement with previous research.[35] Because the asphericity parameter of PAMAM dendrimer is so small, this indicates that the shape of pristine PAMAM dendrimer is spherical. For PAMAM−AuNP composites, these parameters are smaller than that of pristine dendrimer, implying the shapes of the dendrimer still possess spherical structures after encapsulating the AuNP. G4 PAMAM/Au_{201} is the closest one to spherical, because the branching fragment of PAMAM is expanded to completely surround the Au_{201} nanoparticle, leading to the disappearance of the internal cavities formed by the branching fragment of PAMAM. In addition, the parameter of G4 PAMAM/Au_{116} is larger than that of G4 PAMAM/Au_{201}, which might be due to the quantities of cavities in the dendrimer. For G4 PAMAM/Au_{405}, the AuNP is too large to be covered by dendrimer, which causes the shape to become irregular. Further information about the internal structure of the dendrimer is discussed in the next paragraph.

To explore the cavity distribution within the interior of the PAMAM dendrimer, the radial number density distribution was used. Figure 4a,b shows the radial number density profiles of a pristine dendrimer and dendrimers with the AuNPs of different sizes, respectively. It should be noted that the origin of pristine dendrimer is from its mass center, while the AuNP mass centers were the origins of the radial number density distribution for G4 PAMAM−AuNP composites. In Figure 4a, the density profile shows several density valleys following the corresponding peaks, and the lower densities at the valleys can be attributed to the distribution of local cavities within the dendrimer, resulting in a porous structure. For PAMAM/Au_{116}, a prominent first peak with a shoulder peak can be seen in Figure 4b, illustrating that the Au_{116}, which is completely covered by the PAMAM dendrimer, integrates with the local cavities to form a much more compact dendrimer structure, resulting in a high density peak. Because the dendrimer can completely encapsulate the Au_{116}, the local density of dendrimer away from the Au_{116} surface is not influenced and forms the shoulder with a local density value close to that of the interior of pristine PAMAM dendrimer. This is a reason why their shapes are so similar, according to the asphericity parameter value shown in Table 4. For PAMAM/Au_{201}, Au_{201} is at a critical size such that the dendrimer can almost completely encapsulate it. The first density peak is wider but lower than that of PAMAM/Au_{116}, and the second density peak

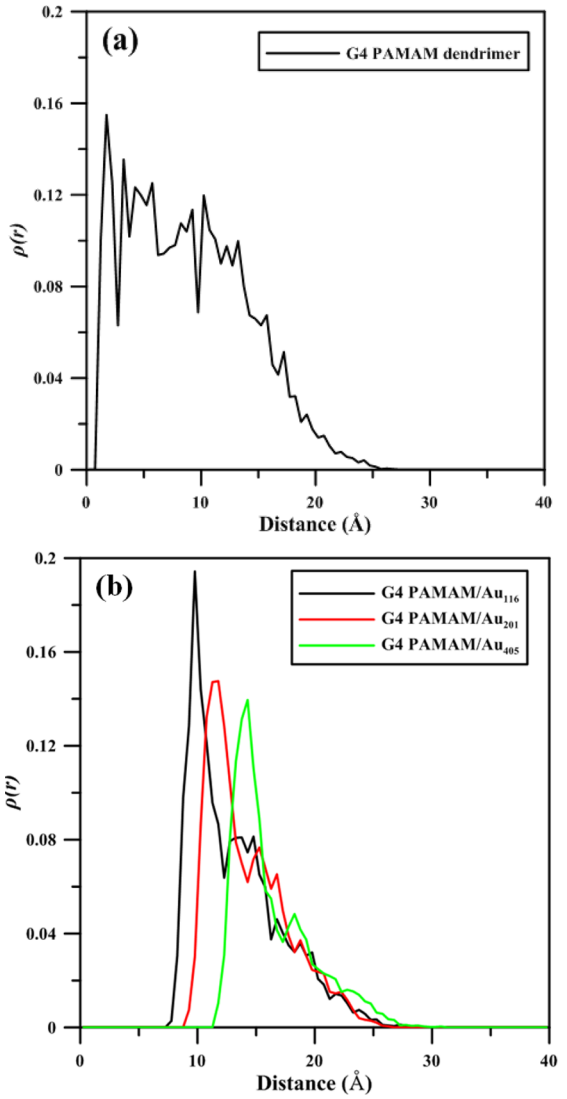

Figure 4. Radial density profile as a function of distance from the center of mass of the (a) G4 PAMAM dendrimer and (b) G4 PAMAM dendrimer/AuNPs.

is slightly lower than that of PAMAM/Au_{116}. For the case of PAMAM/Au_{405}, this AuNP is too large to be encapsulated by the dendrimer. Consequently, the end branches of the dendrimer will extend to envelop the Au_{405}, and the cavities within the pristine dendrimer are extruded, resulting in the disappearance of the shoulder peak.

The synthesized metal nanoparticles within the dendrimer matrix generally possess higher melting temperatures than the degradation temperature of the dendrimer. To obtain nanoparticle thin film from the nanoparticle/dendrimer composites, previous studies used a calcining method on the composites at high temperatures up to 750 K to remove the dendrimers.[22,23] Since it is very difficult to directly observe the dynamical behaviors of the metal nanoparticle and the dendrimer during the temperature elevation process, MD simulation was used again to investigate the dynamical behaviors of the AuNPs and

DOI: 10.1021/acs.iecr.5b02382
Ind. Eng. Chem. Res. 2015, 54, 11560−11567

PAMAM dendrimer as well as the thermal stability of AuNPs. For all AuNP/PAMAM cases, the system temperature was increased from 298 to 1200 K with a heating rate of 2.25 K/ps. For comparison, the simulation results of the corresponding bare AuNPs during the temperature elevation process are also shown.

Figure 5 shows the variations of the binding energy between gold atoms for different sizes of bare AuNPs and PAMAM-encapsulated AuNPs during the temperature elevation procedure. The binding energy is defined as the potential energy of an AuNP divided by the corresponding Au atom number, which can reflect the interaction strength between two Au atoms. At 298 K, one can see that the binding energies of bare AuNPs are more stable than those of the PAMAM-encapsulated AuNPs for all cases, implying the surface atoms of PAMAM-encapsulated AuNPs are slightly distorted after encapsulation by the PAMAM dendrimer. The binding energy profiles basically increase proportionally until the melting temperature, at which the discontinuity of the binding energy profile appears. The predicted melting points of Au_{116}, Au_{201}, and Au_{405} from Figure 5a–c are about 590, 780, and 840 K, respectively. It is obvious that the melting point of AuNP at this size range significantly depends on the AuNP size. These results can be also seen in previous related simulation and experiment studies.[38,39] Consequently, MD simulation by the tight-binding potential can basically reflect the AuNP size effect on the melting point. For the PAMAM-encapsulated AuNPs, the predicted melting points from the temperatures at the discontinuities of the energy profiles are about 670, 805, and 910 K for Au_{116}, Au_{201}, and Au_{405}, respectively. These results indicate that the melting points of dendrimer-stabilized AuNPs are significantly higher than those of the corresponding bare AuNPs. This is because the interaction between the dendrimer and AuNPs limits the expansion of the AuNPs, in effect stabilizing them at higher temperatures.

Configurations of AuNPs at room temperature and the melting point are also displayed in Figure 5. The atomic local shear strain of individual atoms introduced by Shimizu et al.[40] was used to monitor the amount of movement relative to all its first neighbor atoms. The detailed definition of atomic local shear strain can be found in ref 41 of this study and is therefore not introduced here. A large atomic local shear strain value indicates an atom is under local plastic and shear deformation, whereas a smaller value implies an atom undergoes a small amount of movement relative to all its first neighbor atoms or the atom is under local elastic deformation. It can be seen in each case that the surface atoms of AuNP with large displacement appear at the melting temperature.

The relative movements of surface and bulk Au atoms were also investigated by the local shear strain at 298 and 670 K for PAMAM/Au_{116}. In Figure 6a, the Au_{116} configurations in side and cross-sectional views are the reference structures for those shown in Figure 6b. At its melting point of 670 K, it can be seen from the side view of Au_{116} that the shape has undergone a considerable change with some surface atoms displaying larger local shear strain values. From the cross-sectional view of Figure 6b, one can see that some bulk Au atoms still possess small local shear strain values, even though the surface atoms have obtained enough energies to make the relative movement to the nearest Au atoms.

In order to investigate the variation in PAMAM dendrimer conformation during the temperature elevation procedure, the profiles of R_g at different temperatures are shown in Figure 7.

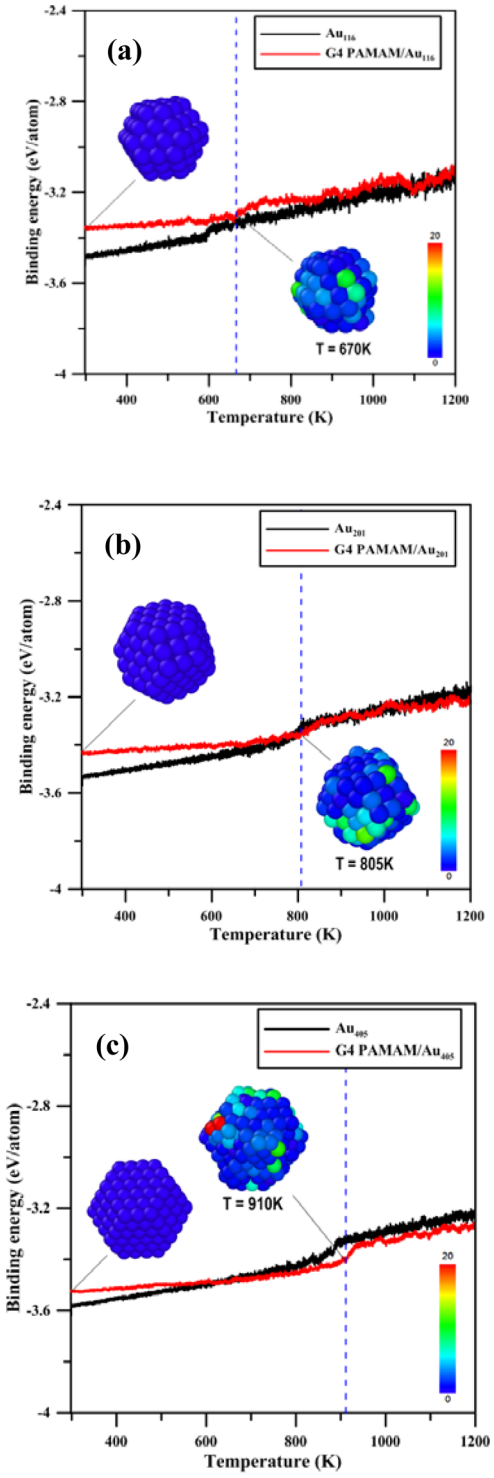

Figure 5. Variations of the binding energies of bare AuNPs and PAMAM dendrimer-encapsulated AuNPs during the temperature elevation procedure for (a) Au_{116}, (b) Au_{201}, and (c) Au_{405}. The local shear strain of AuNPs at room temperature and the melting point are also shown in the inset.

For dendrimers with AuNPs, the R_g values increase roughly linearly with increasing temperature from 298 to 600 K. At temperature higher than 600 K, the R_g values increase more significantly with the increasing temperature; at temperatures higher than the melting points of AuNPs, the R_g values change considerably, indicating the dendrimers undergo significant

DOI: 10.1021/acs.iecr.5b02382
Ind. Eng. Chem. Res. 2015, 54, 11560–11567

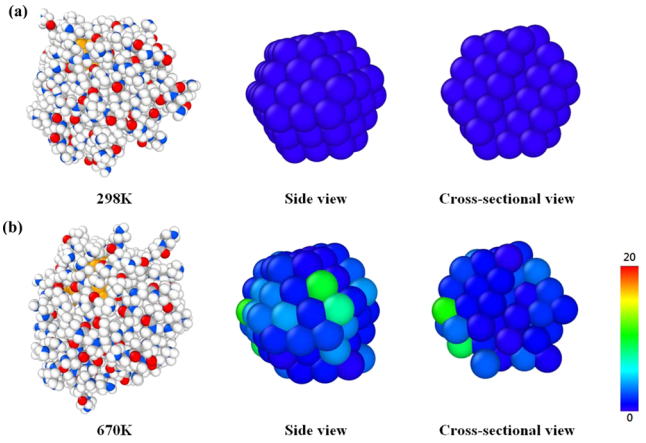

Figure 6. Local shear strain of PAMAM/Au_{116} in side and cross-sectional views at (a) 298 K and (b) 670 K.

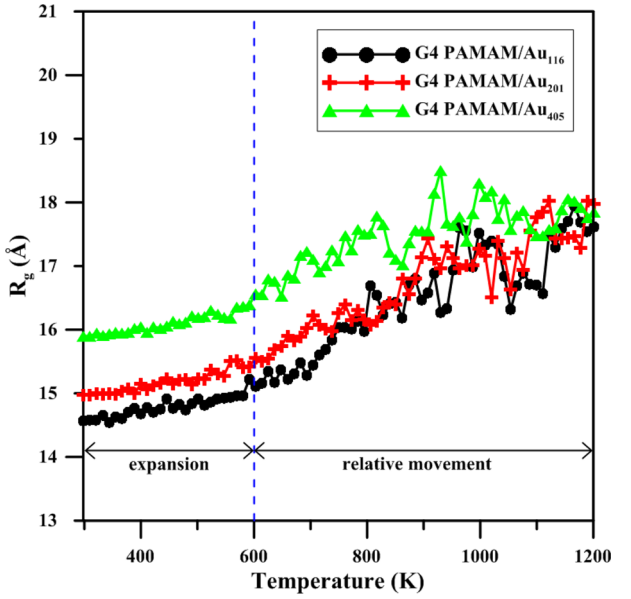

Figure 7. Radius of gyration of PAMAM–AuNP composites during the temperature elevation procedure.

conformation variations. From these simulation results, it can be concluded that the PAMAM dendrimer conducts the thermal expansion when the temperature increases from 298 K to about 600 K. At temperatures higher than 600 K, the dendrimer has enough kinetic energy to overcome the interaction strength between the dendrimer and AuNP, resulting in a prominent increase of R_g value. As the system temperature exceeds the AuNP melting points, the structures of AuNPs are unstable and the shapes of AuNPs display significant changes with the simulation time, which enhances the conformation variations of the dendrimer.

Figure 8 displays the variations of the distance between the mass centers of the PAMAM dendrimer and that of the AuNP at different temperatures. At room temperature, the Au_{116} and Au_{201} are completely encapsulated by the dendrimer, and the mass center distances of these two are very similar. For the Au_{405} partially covered by the dendrimer, the mass center distance is longer. Severe oscillation can be clearly seen in all profiles when the temperature exceeds 600 K, while the mass center distances increase slightly as the temperature increases

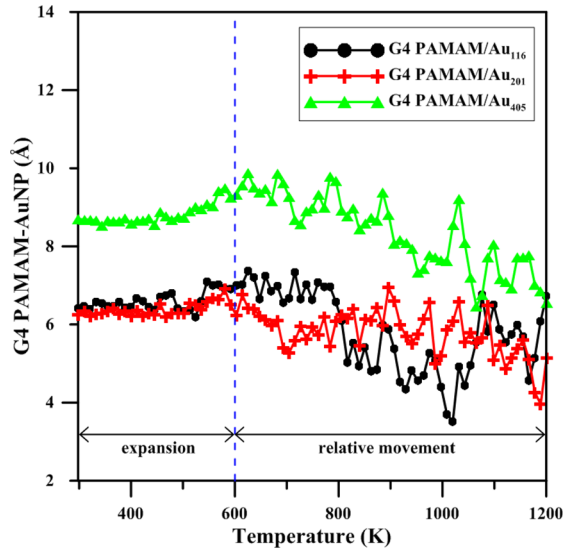

Figure 8. Distance between the center of mass of PAMAM dendrimer and AuNP as a function of temperature.

from 298 to 600 K. This result also confirms the linear increases of R_g values from 298 to 600 K, where the dendrimer only conducts the thermal expansion. When the temperature is higher than 600 K, the kinetic dendrimer energies are high enough to overcome the interaction between the dendrimer and AuNP, resulting in considerable relative movement. In Figure 7, the dendrimers become more extended at higher temperature because of the larger R_g values, while, on the other hand, the mass center distances become smaller at temperatures higher than 600 K. Thus, the dendrimer layer covering the AuNP becomes thinner and more compact at higher temperatures.

In order to observe the dynamical behaviors of PAMAM/AuNPs during the heating process, the square displacement (SD) at different temperatures was used for PAMAM dendrimer and AuNP, respectively. The SD at temperature T is defined by a function of T as shown in eq 4:[42]

$$\mathrm{SD}(T) = \frac{\sum_i^N [r_i(T) - r_i(T_0)]^2}{N} \quad (4)$$

where $r_i(T)$ represents the position of the atom i of dendrimer or AuNP at system temperature T, and $r_i(T_0)$ indicates the referenced position of the corresponding atom at the referenced system temperature T_0. N represents the total atom numbers of dendrimer or AuNP in the investigated system.

Figure 9 shows the SD profiles of the PAMAM dendrimer and AuNP atoms at temperatures from 298 to 1200 K. It is clear that the SD values of the PAMAM dendrimer increase linearly with temperature increases from 298 to 600 K. Conversely, Au SD profiles remain almost zero throughout this temperature range, indicating the slow mobility of Au atoms. Once the system temperature is higher than 600 K, abrupt increases in the dendrimer SD values can be clearly seen in Figure 9, indicating the atoms of the PAMAM dendrimer possess enough kinetic energy to leave their equilibrium positions interacting with the AuNPs and conduct the diffusion. For AuNPs, the SD profiles begin to display prominent increases as the temperature exceeds their respective melting points.

DOI: 10.1021/acs.iecr.5b02382
Ind. Eng. Chem. Res. 2015, 54, 11560–11567

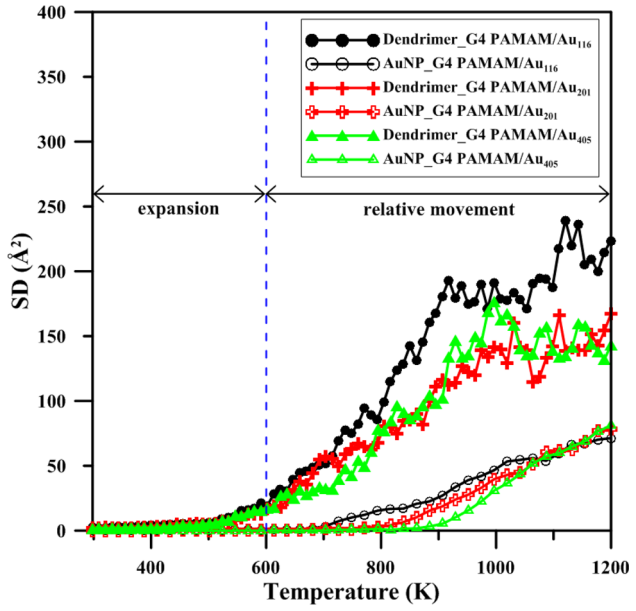

Figure 9. Square displacement profile of the PAMAM dendrimer and AuNP atoms at different temperatures.

4. CONCLUSIONS

In this work, we have used molecular dynamics simulations to study the interactions between G4 PAMAM dendrimers and AuNPs of different sizes in a dry environment. The calculated radius of gyration and the asphericity parameter of pristine PAMAM dendrimers are in good agreement with related previous studies. Our results show that AuNPs will be stabilized within the G4 PAMAM dendrimer, with the irregularity of the surface and the coverage ratio decreasing as the size of the AuNP increases. The branching chains of the dendrimer are no longer able to wrap around the AuNP when its diameter is larger than 2.0 nm. The cavity structure in the PAMAM dendrimer is the critical factor allowing for the AuNP to be encapsulated, and the conformation of G4 PAMAM dendrimer will still possess its unique spherical structure after encapsulating the AuNP. According to thermal stability analysis, the melting points of PAMAM dendrimer-encapsulated AuNP nanoparticles increase significantly when compared to bare AuNPs of the same size. Therefore, if we consider that the degradation temperature of a G4 PAMAM dendrimer is about 500−800 K[43−46] and the diameter of the AuNP is smaller than 1.5 nm, its melting point will increase when it is fully covered by PAMAM dendrimer. When the diameter is larger than 2.0 nm, the AuNP can be removed from the dendrimer via a heating process. Moreover, we found that the PAMAM dendrimer conducts thermal expansion when temperature increases from 298 K to about 600 K. At temperatures higher than 600 K, the dendrimer will move relative to the AuNP. This study helps clarify the characteristics and phenomena of PAMAM−AuNP composites, as well as contributing to the design of new catalysts and nanosensors. Although the PAMAM degradation mechanism cannot be directly simulated in the current study because of the limitation of the CVFF potential, the degradation temperature can still be estimated at the temperature of about 600 K at which the configuration of PAMAM begins significant change. The predicted degradation temperature of PAMAM about 600 K is in agreement with those in the previous experimental studies. Because a lot of applications of PAMAM−AuNP composites are conducted in the solvent environment, it is worth conducting a further study for the behaviors of G4 PAMAM-encapsulated AuNP in the solvent environment in the future.

AUTHOR INFORMATION

Corresponding Author

*Shin-Pon Ju: jushin-pon@mail.nsysu.edu.tw.

Author Contributions

#(H.-L.C. and C.-H.S.) Both authors contributed equally to this work.

Notes

The authors declare no competing financial interest.

ACKNOWLEDGMENTS

The authors would like to thank the (1) Ministry of Science and Technology of Taiwan, under Grant No. MOST 101-2221-E-110-100-MY3, (2) Aim for the Top 500 Universities Grant under the Grant No. NSYSUKMU104-104-P011 from Kaohsiung Medical University for their support on this study, and (3) financial supports by the Chinese Culture University.

REFERENCES

(1) Niu, Y. H.; Crooks, R. M. Dendrimer-encapsulated metal nanoparticles and their applications to catalysis. *C. R. Chim.* **2003**, *6*, 1049−1059.

(2) Quinn, B. M.; Liljeroth, P.; Ruiz, V.; Laaksonen, T.; Kontturi, K. Electrochemical resolution of 15 oxidation states for monolayer protected gold nanoparticles. *J. Am. Chem. Soc.* **2003**, *125*, 6644−6645.

(3) Rao, C. N. R.; Kulkarni, G. U.; Thomas, P. J.; Edwards, P. P. Size-dependent chemistry: Properties of nanocrystals. *Chem. - Eur. J.* **2002**, *8*, 28−35.

(4) Daniel, M. C.; Astruc, D. Gold nanoparticles: Assembly, supramolecular chemistry, quantum-size-related properties, and applications toward biology, catalysis, and nanotechnology. *Chem. Rev.* **2004**, *104*, 293−346.

(5) Hu, M.; Chen, J.; Li, Z.-Y.; Au, L.; Hartland, G. V.; Li, X.; Marquez, M.; Xia, Y. Gold nanostructures: engineering their plasmonic properties for biomedical applications. *Chem. Soc. Rev.* **2006**, *35*, 1084−1094.

(6) Hvolbaek, B.; Janssens, T. V. W.; Clausen, B. S.; Falsig, H.; Christensen, C. H.; Norskov, J. K. Catalytic activity of Au nanoparticles. *Nano Today* **2007**, *2*, 14−18.

(7) Esumi, K.; Miyamoto, K.; Yoshimura, T. Comparison of PAMAM-Au and PPI-Au nanocomposites and their catalytic activity for reduction of 4-nitrophenol. *J. Colloid Interface Sci.* **2002**, *254*, 402−405.

(8) Li, H.; Zheng, Z.; Cao, M.; Cao, R. Stable gold nanoparticle encapsulated in silica-dendrimers organic-inorganic hybrid composite as recyclable catalyst for oxidation of alcohol. *Microporous Mesoporous Mater.* **2010**, *136*, 42−49.

(9) McCaffrey, R.; Long, H.; Jin, Y.; Sanders, A.; Park, W.; Zhang, W. Template Synthesis of Gold Nanoparticles with an Organic Molecular Cage. *J. Am. Chem. Soc.* **2014**, *136*, 1782−1785.

(10) Mariscal, M. M.; Olmos-Asar, J. A.; Gutierrez-Wing, C.; Mayoral, A.; Yacaman, M. J. On the atomic structure of thiol-protected gold nanoparticles: a combined experimental and theoretical study. *Phys. Chem. Chem. Phys.* **2010**, *12*, 11785−11790.

(11) Nemanashi, M.; Meijboom, R. Synthesis and characterization of Cu, Ag and Au dendrimer-encapsulated nanoparticles and their application in the reduction of 4-nitrophenol to 4-aminophenol. *J. Colloid Interface Sci.* **2013**, *389*, 260−267.

(12) Myers, V. S.; Weir, M. G.; Carino, E. V.; Yancey, D. F.; Pande, S.; Crooks, R. M. Dendrimer-encapsulated nanoparticles: New synthetic and characterization methods and catalytic applications. *Chem. Sci.* **2011**, *2*, 1632−1646.

DOI: 10.1021/acs.iecr.5b02382
Ind. Eng. Chem. Res. 2015, 54, 11560−11567

(13) Crooks, R. M.; Zhao, M. Q.; Sun, L.; Chechik, V.; Yeung, L. K. Dendrimer-encapsulated metal nanoparticles: Synthesis, characterization, and applications to catalysis. *Acc. Chem. Res.* **2001**, *34*, 181−190.
(14) Garcia-Martinez, J. C.; Lezutekong, R.; Crooks, R. M. Dendrimer-encapsulated Pd nanoparticles as aqueous, room-temperature catalysts for the Stille reaction. *J. Am. Chem. Soc.* **2005**, *127*, 5097−5103.
(15) Grabchev, I.; Qian, X. H.; Bojinov, V.; Xiao, Y.; Zhang, W. Synthesis and photophysical properties of 1,8-naphthalimide-labelled PAMAM as PET sensors of protons and of transition metal ions. *Polymer* **2002**, *43*, 5731−5736.
(16) Zhang, Z.; Yang, W.; Wang, J.; Yang, C.; Yang, F.; Yang, X. A sensitive impedimetric thrombin aptasensor based on polyamidoamine dendrimer. *Talanta* **2009**, *78*, 1240−1245.
(17) Svenson, S.; Tomalia, D. A. Commentary - Dendrimers in biomedical applications - reflections on the field. *Adv. Drug Delivery Rev.* **2005**, *57*, 2106−2129.
(18) Wang, X.; Cai, X.; Hu, J.; Shao, N.; Wang, F.; Zhang, Q.; Xiao, J.; Cheng, Y. Glutathione-Triggered "Off-On" Release of Anticancer Drugs from Dendrimer-Encapsulated Gold Nanoparticles. *J. Am. Chem. Soc.* **2013**, *135*, 9805−9810.
(19) Shi, X.; Wang, S.; Meshinchi, S.; Van Antwerp, M. E.; Bi, X.; Lee, I.; Baker, J. R., Jr. Dendrimer-entrapped gold nanoparticles as a platform for cancer-cell targeting and Imaging. *Small* **2007**, *3*, 1245−1252.
(20) Crespilho, F. N.; Zucolotto, V.; Brett, C. M. A.; Oliveira, O. N., Jr.; Nart, F. C. Enhanced charge transport and incorporation of redox mediators in layer-by-layer films containing PAMAM-encapsulated gold nanoparticles. *J. Phys. Chem. B* **2006**, *110*, 17478−17483.
(21) Su, P.-G.; Tzou, W.-H. Low-humidity sensing properties of PAMAM dendrimer and PAMAM-Au nanoparticles measured by a quartz-crystal microbalance. *Sens. Actuators, A* **2012**, *179*, 44−49.
(22) Kuhn, M.; Jeschke, J.; Schulze, S.; Hietschold, M.; Lang, H.; Schwarz, T. Dendrimer-stabilized bimetallic Pd/Au nanoparticles: Preparation, characterization and application to vinyl acetate synthesis. *Catal. Commun.* **2014**, *57*, 78−82.
(23) Scott, R. W. J.; Wilson, O. M.; Crooks, R. M. Titania-supported Au and Pd composites synthesized from dendrimer-encapsulated metal nanoparticle precursors. *Chem. Mater.* **2004**, *16*, 5682−5688.
(24) Lee, O.-S.; Schatz, G. C. Molecular Dynamics Simulation of DNA-Functionalized Gold Nanoparticles. *J. Phys. Chem. C* **2009**, *113*, 2316−2321.
(25) Li, T. I. N. G.; Sknepnek, R.; Macfarlane, R. J.; Mirkin, C. A.; Olvera de la Cruz, M. O. Modeling the Crystallization of Spherical Nucleic Acid Nanoparticle Conjugates with Molecular Dynamics Simulations. *Nano Lett.* **2012**, *12*, 2509−2514.
(26) Lane, J. M. D.; Grest, G. S. Assembly of responsive-shape coated nanoparticles at water surfaces. *Nanoscale* **2014**, *6*, 5132−5137.
(27) Mandal, T.; Kumar, M. V. S.; Maiti, P. K. DNA Assisted Self-Assembly of PAMAM Dendrimers. *J. Phys. Chem. B* **2014**, *118*, 11805−11815.
(28) Shi, X.; Lee, I.; Baker, J. R., Jr. Acetylation of dendrimer-entrapped gold and silver nanoparticles. *J. Mater. Chem.* **2008**, *18*, 586−593.
(29) Mandal, T.; Dasgupta, C.; Maiti, P. K. Engineering Gold Nanoparticle Interaction by PAMAM Dendrimer. *J. Phys. Chem. C* **2013**, *117* (26), 13627−13636.
(30) Accelrys. Materials-Studio. Available via the Internet at http://accelrys.com/products/materials-studio/, accessed October 11, 2013.
(31) Plimpton, S. Fast Parallel Algorithms for Short-Range Molecular Dynamics. *J. Comput. Phys.* **1995**, *117*, 1−19.
(32) Hagler, A. T.; Lifson, S.; Dauber, P. Consistent force field studies of intermolecular forces in hydrogen-bonded crystals. 2. A benchmark for the objective comparison of alternative force fields. *J. Am. Chem. Soc.* **1979**, *101*, 5122−5130.
(33) Goyhenex, C.; Bulou, H. Theoretical insight in the energetics of Co adsorption on a reconstructed Au(111) substrate. *Phys. Rev. B: Condens. Matter Mater. Phys.* **2001**, *63*, 235404.
(34) Heinz, H.; Vaia, R. A.; Farmer, B. L.; Naik, R. R. Accurate Simulation of Surfaces and Interfaces of Face-Centered Cubic Metals Using 12−6 and 9−6 Lennard-Jones Potentials. *J. Phys. Chem. C* **2008**, *112*, 17281−17290.
(35) Maiti, P. K.; Li, Y.; Cagin, T.; Goddard, W. A., III Structure of polyamidoamide dendrimers up to limiting generations: A mesoscale description. *J. Chem. Phys.* **2009**, *130*, 144902.
(36) Lee, I.; Athey, B. D.; Wetzel, A. W.; Meixner, W.; Baker, J. R. Structural molecular dynamics studies on polyamidoamine dendrimers for a therapeutic application: Effects of pH and generation. *Macromolecules* **2002**, *35*, 4510−4520.
(37) Rudnick, G.; Gaspari, G. The asphericity of random walks. *J. Phys. A: Math. Gen.* **1986**, *19*, 191−193.
(38) Reich, M.; Utsunomiya, S.; Kesler, S. E.; Wang, L.; Ewing, R. C.; Becker, U. Thermal behavior of metal nanoparticles in geologic materials. *Geology* **2006**, *34*, 1033−1036.
(39) Wang, N.; Rokhlin, S. I.; Farson, D. F. Nonhomogeneous surface premelting of Au nanoparticles. *Nanotechnology* **2008**, *19*, 415701.
(40) Shimizu, F.; Ogata, S.; Li, J. Theory of shear banding in metallic glasses and molecular dynamics calculations. *Mater. Trans.* **2007**, *48*, 2923−2927.
(41) Wang, J.; Hodgson, P. D.; Zhang, J.; Yan, W.; Yang, C. Effects of pores on shear bands in metallic glasses: A molecular dynamics study. *Comput. Mater. Sci.* **2010**, *50*, 211−217.
(42) Dietrich, C.; Bagatolli, L. A.; Volovyk, Z. N.; Thompson, N. L.; Levi, M.; Jacobson, K.; Gratton, E. Lipid rafts reconstituted in model membranes. *Biophys. J.* **2001**, *80*, 1417−1428.
(43) Fadhel, B.; Hearn, M.; Chaffee, A. CO2 adsorption by PAMAM dendrimers: Significant effect of impregnation into SBA-15. *Microporous Mesoporous Mater.* **2009**, *123*, 140−149.
(44) Pan, B. F.; Gao, F.; Gu, H. C. Dendrimer modified magnetite nanoparticles for protein immobilization. *J. Colloid Interface Sci.* **2005**, *284*, 1−6.
(45) Pan, B. F.; Cui, D. X.; Gao, F.; He, R. Growth of multi-amine terminated poly(amidoamine) dendrimerson the surface of carbon nanotubes. *Nanotechnology* **2006**, *17*, 2483−2489.
(46) Cheng, Y.; Xu, T.; he, P. H. Polyamidoamine dendrimers as curing agents: The optimum polyamidoamine concentration selected by dynamic torsional vibration method and thermogravimetric analyses. *J. Appl. Polym. Sci.* **2007**, *103*, 1430−1434.

DOI: 10.1021/acs.iecr.5b02382
Ind. Eng. Chem. Res. 2015, 54, 11560−11567